Applied Catalysis B: Environmental 170-171 (2015) 153–161

Contents lists available at ScienceDirect

Applied Catalysis B: Environmental

journal homepage: www.elsevier.com/locate/apcatb

Nanostructured N-doped TiO_2 coated on glass spheres for the photocatalytic removal of organic dyes under UV or visible light irradiation

V. Vaiano*, O. Sacco, D. Sannino, P. Ciambelli

University of Salerno, Department of Industrial Engineering, Via Giovanni Paolo II 132, 84084 Fisciano, SA, Italy

ARTICLE INFO

Article history:
Received 14 December 2014
Received in revised form 22 January 2015
Accepted 30 January 2015
Available online 2 February 2015

Keywords:
N-doped TiO_2 sol–gel synthesis
Dip-coating process
Glass spheres
Photocatalysis
Organic dyes

ABSTRACT

For the applications of photocatalytic processes aimed to the removal of pollutants from wastewater, slurry reactors that employ aqueous suspension of titanium dioxide nanoparticles are not suitable due to the inconvenient and expensive separation of photocatalyst from treated wastewater. To overcome this drawback, the nanosized titanium dioxide needs to be immobilized on a transparent support.

In the present paper, recyclable visible-light active N-doped TiO_2 photocatalyst was immobilized on glass spheres using a simple sol–gel method. The decrease of N-doped TiO_2 crystallites size was obtained with the addition of Triton X-100 as surface-active agent. The effect of sol–gel synthesis temperature was investigated on the crystallization and crystallites size of N-doped TiO_2 obtaining that the best temperature for the immobilization through dip-coating process was found at −20 °C.

The removal of methylene blue (MB) and eriochrome black-T (EBT) in aqueous solutions was tested to evaluate the photocatalytic activity of the immobilized photocatalyst. The optimization of N-doped TiO_2 amount on glass spheres was evaluated using MB as model pollutant. In particular, it was found that until four dip-coating steps, the photocatalytic activity increased. Moreover, the N-doped TiO_2 immobilized on glass spheres (NDc) can be easily separated from the reaction mixture, and maintained excellent photocatalytic activity and durability after four cycles. Finally, NDc showed a high photocatalytic activity in the decolorization and mineralization of MB and EBT both under UV and visible light irradiation.

1. Introduction

Textile wastewater consists of dyes, pigments, pharmaceutical products, industrial chemicals and various organic compounds [1–3]. Each year, it is estimated that 12% of synthetic textile dyes such as indigo red, rhodamine B, methylene blue (MB), eriochrome black-T (EBT) and methyl orange (MO), are lost during manufacture and processing operations, and 20% of these lost dyes enter into the environment through effluents derived from the treatment process of industrial wastewaters. With increasing synthetic dyes usage, dye removal from wastewater becomes an important but challenging area of research since most of dyes and their degradation products may be carcinogenic and toxic to mammals [4,5].

For the removal of dyes, conventional chemical and biological treatments have been applied but these processes are rather ineffective. In this context, one possible solution could be an adsorption treatment over biodegradable materials [6,7] since it is economically feasible [8] with respect to the most commonly used adsorbent such as activated carbon [9].

Also if the adsorption leads to the removal of dyes from wastewater, when the saturated adsorbent material is dumped into the land, it pollutes again the air and soil creating secondary pollution.

As promising alternative, heterogeneous photocatalysis using semiconductors could be used for wastewater treatment because it leads to the complete mineralization or detoxification of dyes to environmental benign CO_2, H_2O, nitrates, etc.

The low cost of catalysts and the utilization of renewable energy associated to this technology, are attractive compared to other techniques [10].

Titanium dioxide (TiO_2) is the photocatalyst widely used in water purification technology [11–15]. However, the main deficiency for the practical applications of TiO_2 is limited by its large band-gap (3.2 eV), meaning that it can be only active under the UV light irradiation [16–21]. The main research objectives are to increase the photocatalytic performances of TiO_2 through the doping of its crystalline structure with non-metal ions that reduces the

* Corresponding author. Tel.: +39 89 964006; fax: +39 89 964057.
E-mail address: vvaiano@unisa.it (V. Vaiano).

http://dx.doi.org/10.1016/j.apcatb.2015.01.039
0926-3373/

band-gap and makes possible the fruitful absorption of the visible light [14,22–31]. It was shown that the doping of TiO_2 with nitrogen has led to an enhanced photocatalytic activity in presence of visible light irradiation [24,28].

However, one of the most important drawbacks of photocatalytic process is that photocatalysts are often used in slurry reactors. The limitation of the slurry process is that the photocatalyst in powder must be separated from the system after the treatment. The cost of this separation step may even invalidate economically the technique [32].

One of the possible solution to this technical problem could be the use of heterogeneous fixed bed reactors, in which the photocatalyst is supported in granular form or as thin film on transparent materials [33].

There is an important variety of materials that can be used for supporting TiO_2. The most studied are that ones based on glass, owing to their low cost and easy availability [34]. For supporting the photocatalysts on these materials, different techniques are developed [35]. The success of these coating processes is based on the large adherence between TiO_2 and glass and to provide a high surface area of TiO_2 deposited. Only few papers regard N-doped TiO_2/immobilized systems mainly carried out through sputtering technique [36], oxidation of TiN thin films [37] and anodization processes [38]. No study developed a simple sol–gel method that uses ammonia solution as the only doping source.

For this reason, the aim of this work was: (i) the immobilization of visible-light active N-doped TiO_2 photocatalyst on glass spheres using a simple sol–gel method; (ii) the optimization of the conditions of sol–gel synthesis for obtaining a high photo-active surface area; (iii) the optimization of the N-doped TiO_2 amount deposited on glass spheres; (iv) the evaluation of photocatalytic activity of the prepared supported photocatalysts in the removal of aqueous solution of MB and EBT both under UV and visible light irradiation.

2. Experimental

2.1. Sol–gel synthesis

Triton X-100 (nonionic surfactant, Sigma–Aldrich) has been used as binder [39]. Triton X-100 was dissolved in isopropyl alcohol (i-PrOH, 99.8 wt%, Sigma–Aldrich) and the pH of solution was adjusted with nitric acid (HNO_3, 65 wt%, Carlo Erba) until to reach a value of about 2. Then, titanium(IV) isopropoxide (TTIP, 97%, Sigma–Aldrich), used as titanium precursor, was added to the mixture.

The use of a low pH limits condensation reactions, imposes a repulsive charge and limits the size of precipitates [40].

In order to investigate the effect of the synthesis temperature on N-doped TiO_2 crystallites size, different synthesis temperatures were used. The investigated temperatures were 0 °C, −5 °C, −15 °C, −20 °C. A cryostat bath was used to control and monitor the temperature during the sol–gel synthesis. Once the solution reached the temperature conditions, an ammonia aqueous solution (30 wt%, Sigma–Aldrich) was added as nitrogen precursor, while the water is able to induce the hydrolysis reaction with TTIP. The molar ratio N/Ti was equal to 18.6 and corresponds to an optimized catalyst formulation found in a previous work [24]. The obtained solution was used for the immobilization of N-doped TiO_2. All prepared samples are reported in Table 1.

Table 1
Synthesis reaction temperature, amount of surface-active agent (Triton X-100), crystallite size, SSA (BET) of different N-doped TiO_2 samples.

Catalyst	Synthesis reaction temperature (°C)	Amount Triton X-100 (g)	TiO_2 average crystallites size (1 0 1) (nm)	SSA (m^2/g)
N–T	0	0	17	30
0 NDc	0	5	9	98
−5NDc	−5	5	8	108
−15NDc	−15	5	7	128
−20NDc	−20	5	6	147

2.2. Immobilization of N-doped TiO_2 on glass spheres

Pyrex spheres (d_p = 4.3 mm, from Microglass Heim) were used as glass substrate for the immobilization of N-doped TiO_2, which has been performed through dip-coating technique.

Before dip-coating, the whole surface of glass spheres was rinsed with MilliQ grade water and calcined at 450 °C for 30 min. N-doped TiO_2 coating (NDc) was realized by immersing the glass spheres in the solution prepared as reported in Section 2.1. The glass spheres were maintained in the solution for 10 min and then calcined for 30 min at 450 °C.

The dip-coating and calcination processes were repeated three, four and six times for finding the best amount N-doped TiO_2 dispersed on the glass spheres surface. All prepared samples are reported in Table 2. The N-doped TiO_2 amount coated on glass spheres has been measured using precision balance (Mettler Toledo).

2.3. Samples characterization

The catalysts were characterized by several techniques. Specific surface area (BET) was evaluated from dynamic N_2 adsorption measurement at −196 °C, performed by a Costech Sorptometer 1040 after pretreatment at 150 °C for 30 min in He flow.

Wide-angle X-ray diffraction (WAXD) patterns with nickel filtered Cu-Kα radiation were obtained with an automatic Bruker D8 advance diffractometer, in reflection. Laser Raman spectra were obtained at room temperature with a dispersive MicroRaman (Invia, Renishaw), equipped with 514 nm diode-laser, in the range 100–2000 cm^{-1} Raman shift on powder and structured samples. Scanning electron microscopy (SEM) (Assing, mod. LEO 420) was used to characterize the morphology of NDc samples at an accelerating voltage of 20 kV. UV–vis DRS spectra of catalysts were recorded by a PerkinElmer spectrophotometer lambda 35 using a RSA-PE-20 reflectance spectroscopy accessory (Labsphere Inc., North Sutton, NH). All spectra were obtained using an 8° sample positioning holder, giving total reflectance relative to a calibrated standard SRS-010-99 (Labsphere Inc., North Sutton, NH). The optical band-gap of each catalyst sample was determined by plotting

Table 2
Number of dip-coating steps; crystallites size, SSA and N-doped TiO_2 amount immobilized on glass spheres.

Catalyst	Number of dip-coating	Synthesis reaction temperature (°C)	N-doped TiO_2 amount (wt%)	TiO_2 average crystallites size (1 0 1) (nm)	SSA (m^2/g)
Glass spheres	0	–	0		0.095
3NDc	3	−20	0.22	6	0.27
4NDc	4	−20	0.34	6	0.42
6NDc	6	−20	0.77	6	1.2

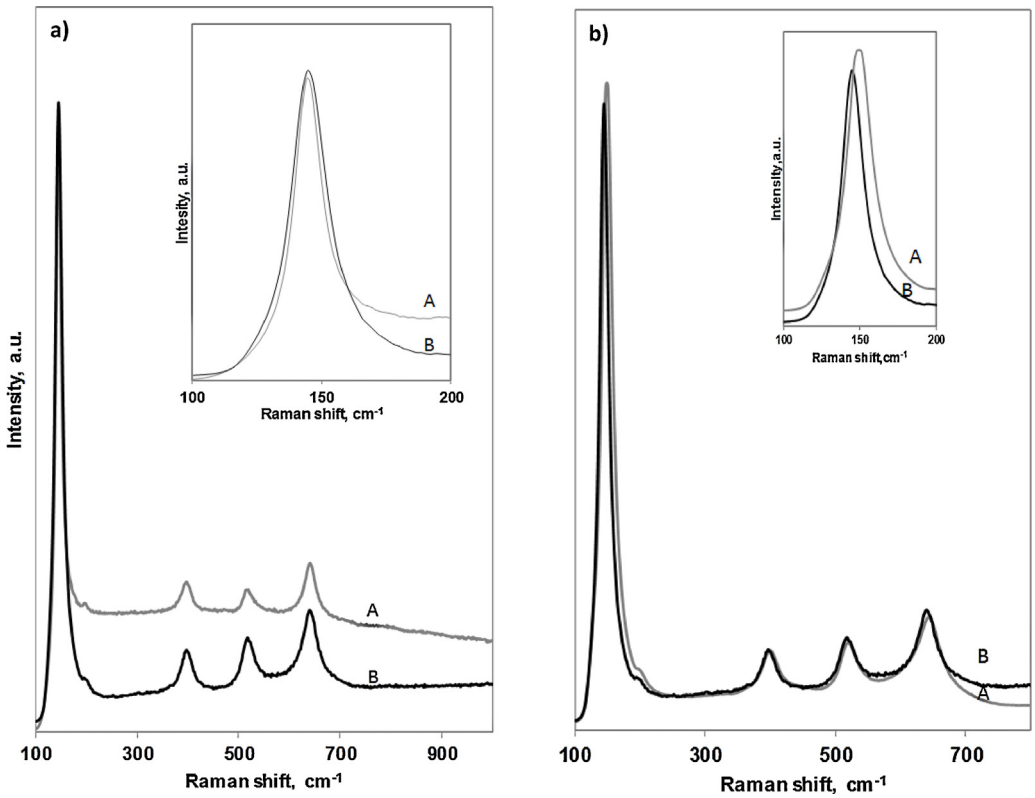

Fig. 1. (a) Raman spectra of (A) N–T synthetized by sol–gel method at 0 °C and (B) 0NDc synthetized by sol–gel method at 0 °C using surface-active agent (Triton X-100); Raman shift of E_g modes in the range 110–200 cm^{-1} (inset). (b) Raman spectra of (A) 0NDc synthetized by sol–gel method using surface-active agent (Triton X-100) at 0 °C and (B) −20NDc synthesized by sol–gel method using surface-active agent (Triton X-100) at −20 °C; Raman shift of E_g modes in the range 100–200 cm^{-1}(inset).

$[F(R_\infty) \times h\nu]^2$ ($F(R_\infty)$) vs $h\nu$ (eV) and calculating the x intercept of a line passing through $0.5 < F(R_\infty) < 0.8$.

2.4. Photocatalytic activity tests

Methylene blue (MB) and eriocrome black-T (EBT) were used as model dyes. The experiments were carried out with the initial concentration of MB and EBT equal to 5 mg/L, at ambient temperature and pressure. The amount of NDc on glass spheres used during the photocatalytic test was equal to 0.4 g/L. The experiments were realized using a pyrex cylindrical photoreactor (I.D = 3 cm) equipped with a peristaltic pump that continuously mix the aqueous solution. Thermocouple was inserted inside the reactor to monitor the temperature during irradiation. As visible light source, a white light LEDs strip (light intensity: 32 mW/cm^2; emission spectrum in the range 400–800 nm) was used and, as UV source, an UV emitting LEDs strip (light intensity: 35 mW/cm^2; emission spectrum in the range 365–400 nm) was utilized. Both LEDs strips are placed surrounding the external body of the cylindrical photoreactor. The schematic picture of experimental set-up is reported in a previous paper [27].

The system was left in dark until reaching MB and EBT adsorption equilibrium, and then photocatalytic reaction was initiated under UV light or visible light.

Liquid samples were analyzed in continuous by spectrophotometric measurement. In particular, a special assembly with a flow quartz cuvette and an external pump for the recirculation of liquid was used, permitting to determine the change of MB and EBT concentration, measured with a PerkinElmer UV–vis spectrophotometer at λ = 663 nm and 528 nm, respectively. A standard calibration curve was obtained for different MB and EBT concentration and allowed to convert absorbance to concentration (mg/L) units. The total organic carbon (TOC) of aqueous samples was measured by the high temperature combustion method on a catalyst (Pt/Al_2O_3) in a tubular flow microreactor operating at 680 °C, with a stream of hydrocarbon free air to oxidize the organic carbon. Laboratory apparatus consisted of mass flow controllers (Brooks) operating on each gas; an injection system; a NDIR continuous analyzer (Hartmann & Braun Uras 10E) for the measurements of CO_2 concentration at the combustion reactor outlet.

3. Results and discussion

3.1. Optimization of N-doped TiO_2 sol–gel synthesis temperature for the coating process

3.1.1. Raman spectra

Raman results are reported in Fig. 1. Fig. 1a presents the comparison between N and T synthesized by sol–gel method without the use of Triton X-100 at 0 °C (a), and at 0 °C in presence of Triton X-100 (b). The Raman spectra of both samples showed bands at 142, 398, 518, 641 cm^{-1} and a weak shoulder at 197 cm^{-1}, which are assigned to the E_g, B_{1g}, A_{1g} or B_{2g} and E_g modes of the anatase phase, respectively [41].

From Fig. 1 (inset), it is easily to see that the strongest Raman signal at 142 cm^{-1}, shifts toward higher wavenumber (144 cm^{-1}). This phenomenon means that the N-doped TiO_2 grains are smaller in size [42].

In Fig. 2b, the effect of different sol–gel synthesis temperatures was also analyzed for 0NDc and −20NDc samples using Triton X-100. In particular, the strongest Raman peak (E_g) at 149 cm^{-1} mode of TiO_2 in the sample 0NDc presents a blue shift up to 144 cm^{-1} for the sample −20NDc. This data indicated that both the use of a

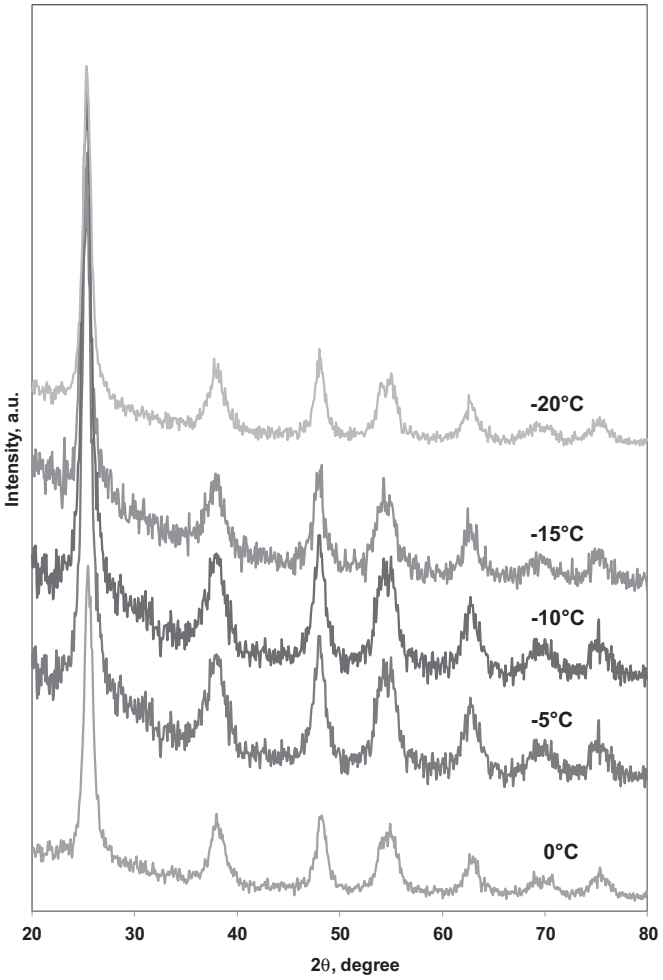

Fig. 2. XRD patters of NDc at different synthesis reaction temperature.

surface-active agent and a synthesis temperature lower than 0 °C lead to the formation of TiO_2 with grains smaller in size [42].

3.1.2. XRD measurements

The results obtained from X-ray diffraction analysis showed the presence of signals typical of the titanium dioxide in the anatase form in all synthesized samples (Fig. 2) [40]. No signals related to rutile phase have been observed.

Furthermore, the average crystallite size of N–T and of all NDc samples was calculated using the Scherrer equation on diffraction plane (1 0 1) and the obtained values are reported in Table 1. Also from XRD analysis, it is possible to observe that the presence of Triton X-100 can effectively prompt the crystallization and inhibits the grain growth allowing to obtain smaller TiO_2 crystallites [42]. In particular, the use of Triton X-100 in the sol–gel synthesis reduces the average crystallites size from 17 to 9 nm. It is well known that the addition of a surface-active agent such as Triton X-100 in the sol–gel synthesis may provide a convenient way to prepare small-sized particles [43]. Generally, nanoparticles are formed in two processes: first, the formation of a large crystal nucleus and secondly, the growth of the nucleus. The surface-active agent was easily adsorbed on the surface of the crystal nucleus and hence probably hindered the further growth of these crystals, and in addition, the adsorption of the surface-active agent may also stabilize the nanoparticles [42].

From Table 1, it is also evident the strong influence of sol–gel synthesis temperature on the final NDc crystallite size.

The kinetics of the sol–gel process based on hydrolysis and condensation reactions of titanium alkoxides (TTIP) are an important parameter for the average crystallites size of final TiO_2. This process generally follows three different steps: the first stage is the formation of hydrolyzed monomers [44]; the second step corresponds to the moment when the concentration of these monomers reached the level of critical supersaturation forming primary particles; the third step is the grow of primary particles by aggregation.

Baros et al. showed that the reaction between TTIP and H_2O in *n*-propanol solution (hydrolysis) is very fast and not influenced by the synthesis temperature.

The formation of titanium-oxo-alkoxy clusters through the alcoxolation reaction is instead influenced by the temperature according to Arrhenius law [45]. The rate of clusters nucleation has decreased by decreasing the temperature. As a consequence, the final size of TiO_2 nanoparticles is lower [45].

Similarly, in the present study, the effect of decreasing the sol–gel synthesis temperature shows that N-doped TiO_2 crystallite size decreases up to about 6 nm when the temperature was equal to −20 °C. Therefore, probably also in presence of ammonia aqueous solution, a lower synthesis temperature inhibited the rate of clusters nucleation.

Fig. 3 illustrates the XRD patterns and UV–vis DRS analysis of −20NDc sample and undoped TiO_2 obtained in the same synthesis conditions but without adding the ammonia aqueous solution.

The diffraction peaks (Fig. 3a) related to (1 0 1) plane of −20NDc sample shifts to a lower value of 2θ (25.29°) with respect to the diffraction peaks at 25.53° (related to the same (1 0 1) plane) of undoped TiO_2. This may be because N replaces O in the TiO_2 structure due to differences in binding properties [46] meaning that the crystalline structure of anatase has been doped with nitrogen. This result has been confirmed by UV–vis DRS spectra (Fig. 3b). Undoped TiO_2 is activated with photons of energy of a longitude close to about 380 nm which involves a band gap in the range 3.3–3.4 eV, typical value for TiO_2 in anatase phase. For the synthesized −20NDc, the doping process determined a decrease of band-gap value from 3.3–3.4 eV to 2.5 eV.

3.1.3. Specific surface area measurements

The surface area of N-doped TiO_2 obtained at different synthesis temperature is shown in Table 1. All the NDc catalysts show a higher surface area with respect to N–T. The higher surface area of NDc catalysts is due to the lower crystallites size caused by the use of Triton X-100. It is also observed that the surface area of the NDc catalysts increases following a linear trend with the decrease of synthesis temperature (Fig. 4). This can be attributed to decrease of the crystallites size, as discussed in XRD analysis (Section 3.1.2).

3.2. Characterization of N-doped TiO_2 immobilized on glass spheres

3.2.1. Raman spectra

The structural properties of the NDc immobilized on glass spheres (Table 2) were investigated by Raman spectroscopy. Fig. 5 displays the Raman spectra of the 3NDc, 4NDc and 6NDc, respectively. All the samples exhibit the characteristic Raman-active modes of the anatase TiO_2 phase [41]. The presence of glass substrate did not change the Raman modes of supported N-doped TiO_2 that are really similar to the Raman modes founded for the −20NDc powder. The N-doped TiO_2 particle size immobilized on glass spheres has been estimated by Raman spectra following the method reported by Kontos et al. [47], finding that the value is about 6 nm, very similar to that one evaluated from XRD data for −20NDc sample in powder form. Thus, these data confirm that dip-coating does not induce a change of N-doped TiO_2 crystallite size.

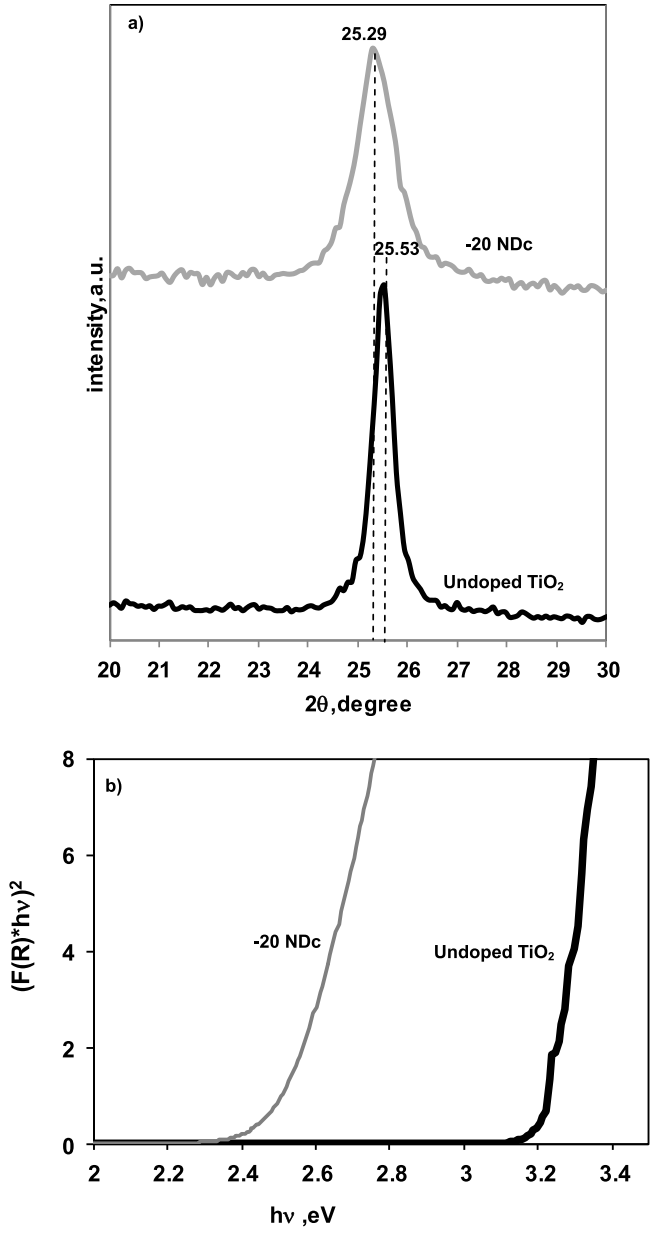

Fig. 3. (a) XRD patters in the 2θ range of 20–30° and (b) UV–vis DRS of undoped TiO_2 and −20NDc samples.

3.2.2. SEM

The surface morphology of NDc photocatalysts immobilized on glass spheres is studied by scanning electron microscopy whose results are presented in Fig. 6. The SEM images demonstrate the presence of N-doped TiO_2 deposited on the surface of glass spheres, and rough surface of the coating, which is necessary for the good photocatalytic activity of the NDc [48]. As shown in Fig. 6, the glass spheres surface (Fig. 6a) appears smooth and without roughness. The first three coating steps (3NDc) are not covering the entire surface. In particular, as showed in the SEM picture in the zone evidence with a circle, there is still a fraction of glass surface not covered by photocatalyst aggregates. Additional dip-coating steps (4NDc and 6NDc) lead to a complete coverage of the glass support.

Therefore, N-doped TiO_2 is more uniformly distributed on the surface of 4NDc and 6NDc as compared to 3NDc (Fig. 6a). However, the sample 6NDc shows N-doped TiO_2 aggregates with higher size compared to 4NDc.

The morphology of N-doped TiO_2 aggregates seems to be as pseudo spherical (Fig. 6b) in all samples and there is no considerable change in morphology for the samples 4NDc and 6NDc. Moreover, SEM images evidence that N-doped TiO_2 aggregates are well dispersed and its distribution covers homogeneously the surface of glass spheres.

4.2.3. Specific surface area measurements

Table 2 presents the BET surface area values for glass spheres, 3NDc, 4NDc and 6NDc. It can be seen that the BET surface area of coated glass spheres increased by a factor of almost 3 for 3NDc and 12 for sample 6NDc as compared to the uncoated glass spheres. This increase in surface area is attributed to the NDc coating which results in a porous and rough surface, as observed from SEM analysis. Thus, the increase in surface area should help in increasing the N-doped TiO_2 exposure to light which in turn would increases the photocatalytic reaction rate.

3.3. Photocatalytic activity tests

3.3.1. Dark adsorption and photolysis of MB and EBT in presence of glass spheres

Prior to the photocatalytic removal, the dark adsorption and the photolysis of MB and EBT in presence of uncoated glass spheres were evaluated. The concentration of MB and EBT was 5 mg L^{-1} for both dyes.

In Fig. 7, the adsorption of dyes was studied by passing each dye solution through glass spheres under dark conditions until it gets the constant value. After 10 min, it was observed a decrease of concentration of dyes, equal to 7 and 5% for MB and EBT, respectively. Then, dyes concentration started to increase, reaching a decrease of 4 and 3% for MB and EBT, respectively, after 30 min and this value was almost the same up to 1 h. The decrease in concentration of dyes was due to the adsorption of dye on the surface of glass spheres.

After the dark period, the solution was irradiated with UV light or visible light. The uncoated glass showed no decolorization activity but only a little dye desorption due to the increase of temperature up to about 35 °C, caused by light sources (Fig. 8). These experimental results evidenced that the glass spheres do not have photocatalytic activity when N-doped TiO_2 is not present on their surface.

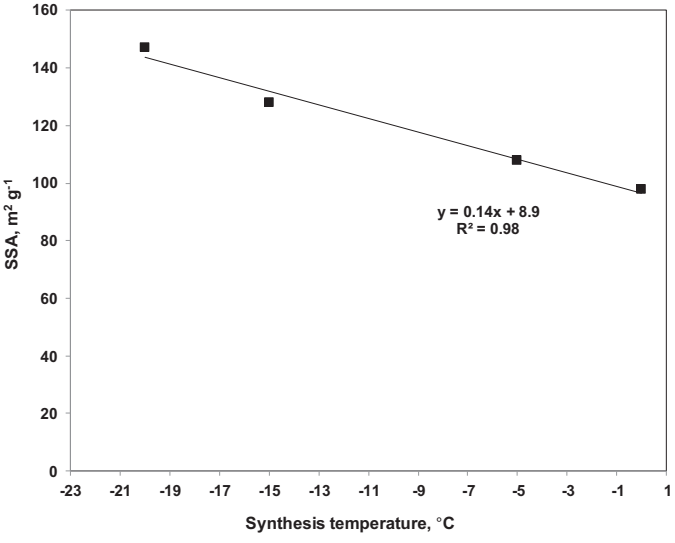

Fig. 4. Trend of NDc specific surface area ($m^2\ g^{-1}$) as a function of sol–gel synthesis reaction temperature.

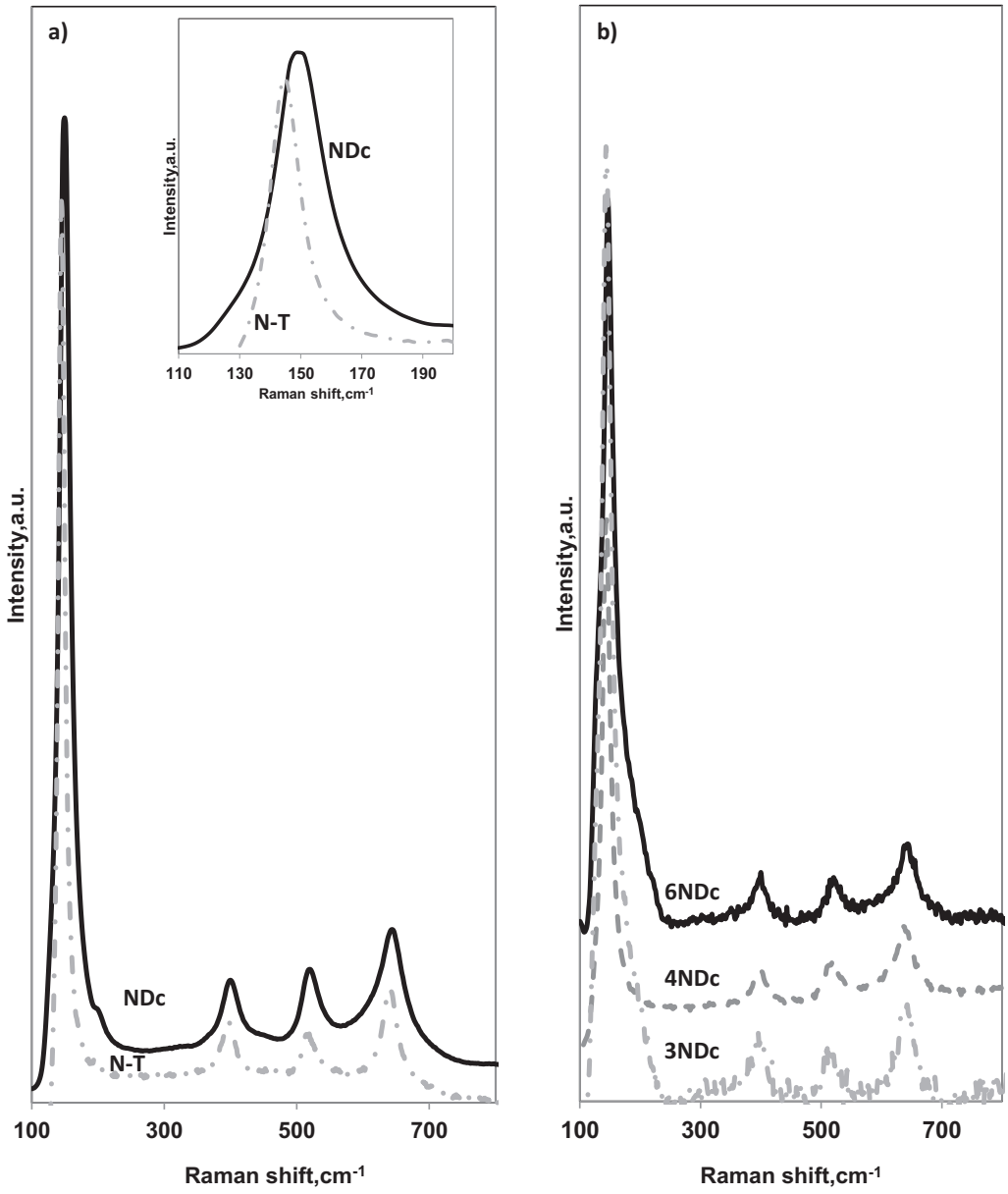

Fig. 5. (a) Raman spectra of N–T and NDc samples in the range of 100–800 cm^{-1} and Raman shift of E_g modes in the range 110–200 cm^{-1} (insert); (b) Raman spectra of NDc on glass spheres in the range of 100–800 cm^{-1}.

3.3.2. Optimization of NDc amount on glass spheres

In order to define the best NDc amount deposited on glass spheres, MB dye has been chosen. In Fig. 9, the comparison of the photocatalytic activity obtained with the 3NDc, 4NDc and 6NDc samples is shown.

Firstly, it was evaluated the decolorization of MB due to the dark adsorption until get the constant value. All structured photocatalysts (3NDc, 4NDc and 6NDc) have an initial step of adsorption corresponding to 20, 33 and 37% of MB decolorization, respectively. After the dark period, the solution was irradiated with UV light and the reaction started to occur. Under UV light irradiation 3NDc, 4NDc and 6NDc catalysts showed a photocatalytic activity leading to an additional MB decolorization of about 20, 46 and 43%, respectively, after 107 min of irradiation time.

These results evidenced that up to NDc amount of 0.34 wt% (4NDc), photocatalytic activity markedly increased indicating that the overall of N-doped TiO_2 nanoparticles dispersed on the surface of glass spheres is effectively irradiated. For NDc amount of 0.77 wt% (6NDc), photocatalytic decolorization rate was almost the same of that one obtained with 4NDc catalyst. This means that the amount of N-doped TiO_2 effectively irradiated did not change because the amount of NDc added after four steps of dip-coating, masks the lower layers of NDc. Thus, the best sample chosen to investigate the stability and the ability to work with visible light irradiation and other types of dyes (EBT) was 4NDc.

3.3.3. Recyclability of 4NDc photocatalyst for decolorization of MB

Recyclability is one of the most important factors in catalysis research. To confirm the recyclability of 4NDc sample, the photocatalytic decolorization reaction was repeated up to four cycles (Fig. 10). The results demonstrated that there was 1–2% reduction

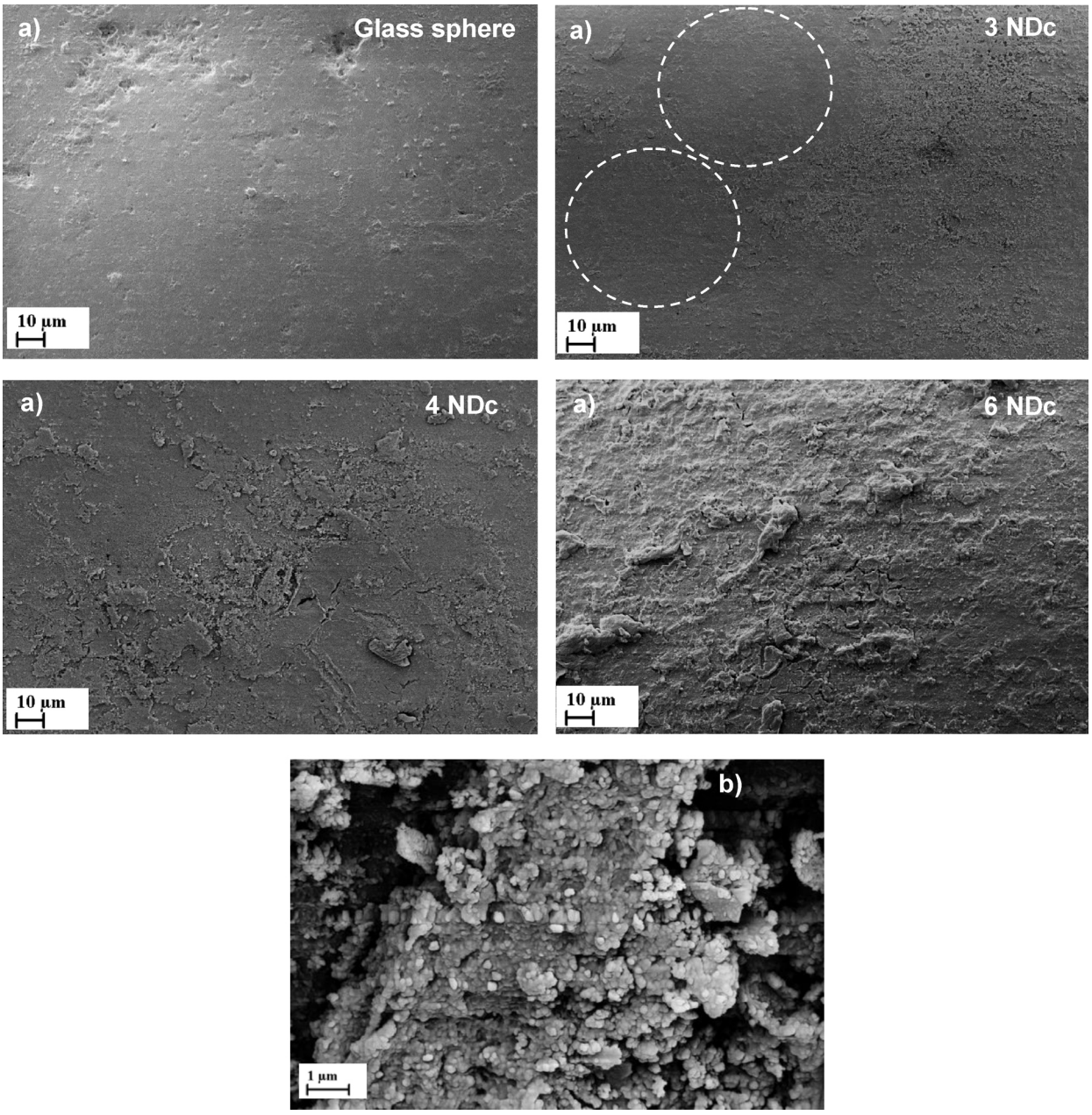

Fig. 6. (a) SEM images of glass sphere, 3NDc, 4NDc and 6NDc; (b) SEM images of morphology of NDc on glass spheres.

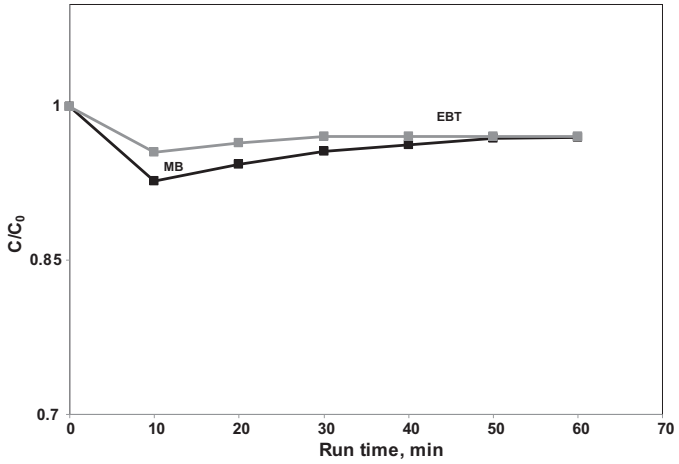

Fig. 7. Dark adsorption of MB and EBT on uncoated glass spheres.

of decolorization percentage in 30 min of irradiation and about 10% in 60 min of irradiation after four cycles, being within the limits of the error bars. The slight decrease in the decolorization rate may be due to the weakening of the dye adsorption ability. These results confirm that the photocatalytic activity of 4NDc was nearly the same indicating that there is no leaching of NDc from coated glass spheres confirmed by the measurement of N-doped TiO_2 amount after photocatalytic tests. These results also confirm the stability of NDc coated on glass spheres.

3.3.4. Photocatalytic activity under UV or visible light irradiation

The 4NDc exhibited high photocatalytic activity also under visible light irradiation, allowing to obtain a decolorization of MB equal to 52% after 210 min of irradiation (Fig. 11). The system is also able to degrade EBT both under visible and UV light obtaining a decolorization of EBT equal to 41% and 31% under UV and visible light, respectively.

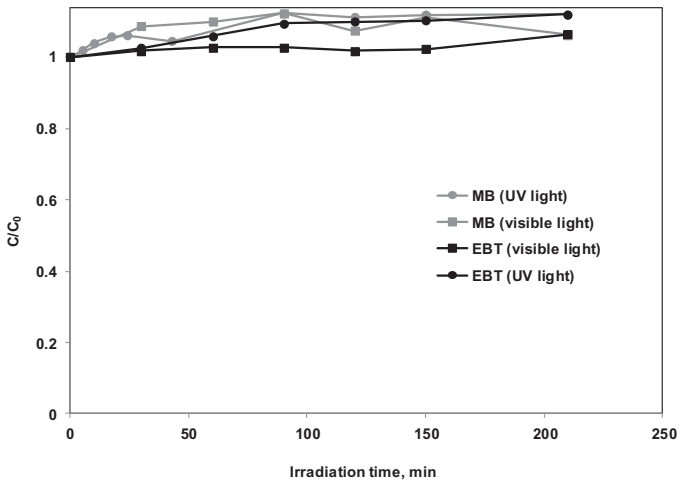

Fig. 8. Photolysis of MB and EBT in presence of uncoated glass spheres under UV and visible light irradiation.

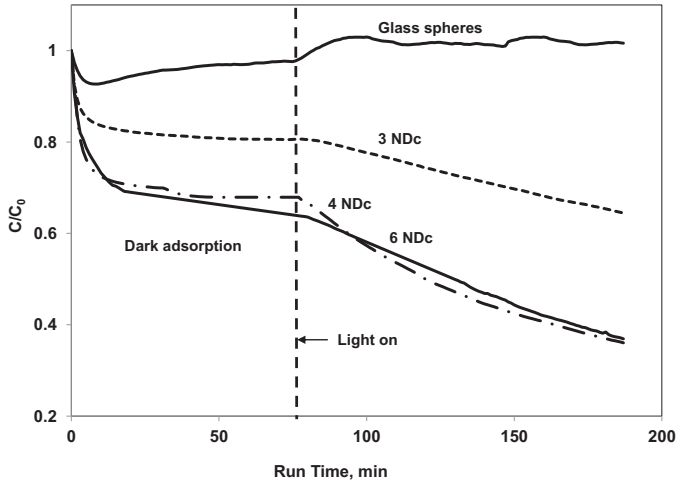

Fig. 9. Photocatalytic decolorization of MB under UV light irradiation (optimization of NDc amount on glass spheres).

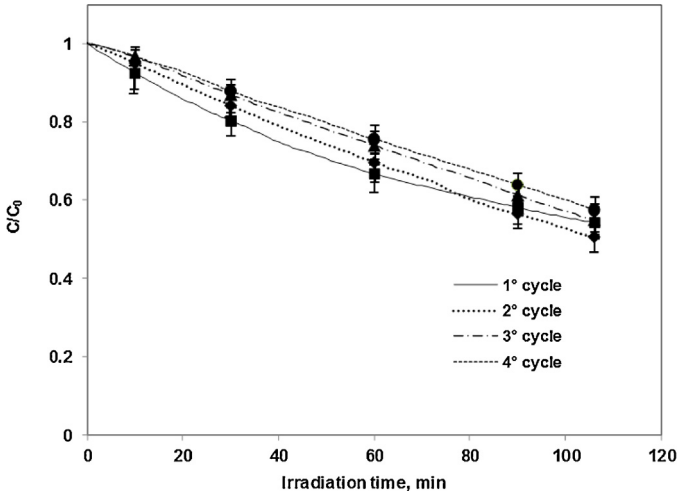

Fig. 10. Evaluation of MB decolorization performances obtained on 4NDc after 4 recycling experiments.

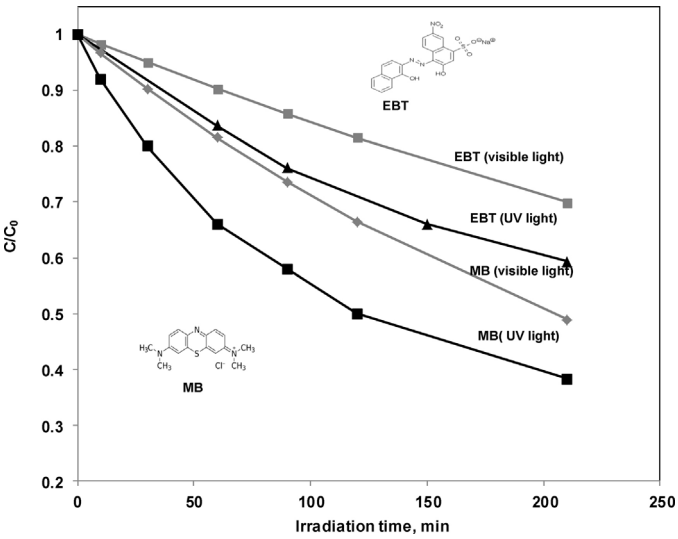

Fig. 11. Photocatalytic decolorization of MB and EBT under UV and visible light irradiation on 4NDc.

It is possible to observe that the photocatalytic MB decolorization activity was higher that one obtained for EBT. The different trend is linked to the different chemical nature of the two dyes. MB is classified as basic dyes due to cationic functional groups such as $-NH_3^+$ [49], while EBT is classified as an azoic dyes due to azo bonds (—N=N—) [49]. The adsorptive affinity of MB on TiO_2 anatase phase is higher than an anionic azo dye, such as EBT; therefore, photocatalytic decolorization activity was quicker for MB [49].

The decolorization does not necessary correspond to the mineralization of the two target dyes. For this reason, the behavior of TOC has been analyzed. The obtained results are reported in Fig. 12. It is possible to observe a progressive decrease of TOC of aqueous sample as a function of irradiation time indicating that 4NDc sample is also able to mineralize MB and EBT both under UV and visible light irradiation.

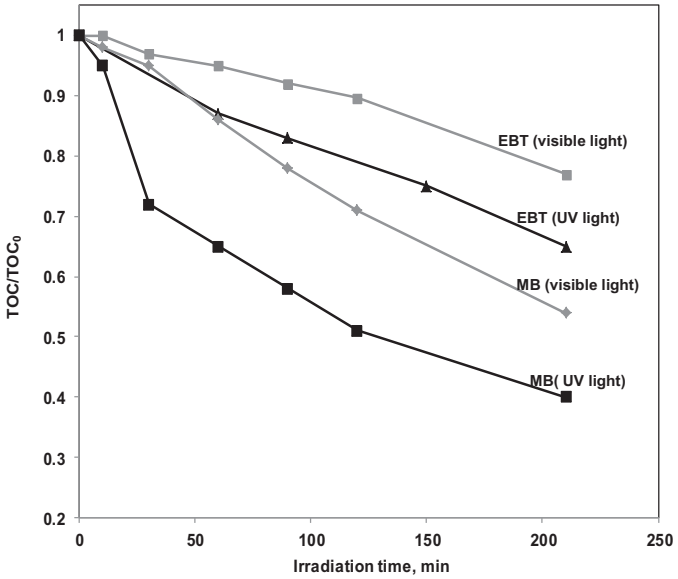

Fig. 12. Photocatalytic mineralization of MB and EBT under UV and visible light irradiation on 4NDc 4NDc.

4. Conclusions

Visible active N-doped TiO_2 (NDc) was successfully immobilized on glass spheres using sol–gel method starting from titanium isopropoxide and ammonia aqueous solution as nitrogen precursor. The first aim of the paper was to obtain the best synthesis condition for increasing the specific surface area of the immobilized NDc. It was found that the sol–gel synthesis temperature has a strong effect on crystallite size during the nucleation step. In particular, the lower the temperature, the lower is the value of NDc crystallite size.

The amount of the NDc on the surface of glass spheres increased with the number of dip-coating steps and varied from almost 0.22 wt% (three coating) to 0.77 wt% (six coatings). The efficiency of structured photocatalysts was evaluated in the decolorization of recalcitrant contaminants like methylene blue, both under UV and visible light irradiation. All the samples showed high photocatalytic activity in decolorization of methylene blue, but the optimal NDc amount was found to be equal to 0.34 wt% obtained after four coatings. This structured photocatalysts still have great catalytic activities after four cycles and were able to remove also erichrome black-T both in presence of UV and of visible light.

References

[1] A.A. Ahmad, B.H. Hameed, N. Aziz, J. Hazard. Mater. 141 (2007) 70–76.
[2] N. Barka, A. Assabbane, A. Nounah, L. Laanab, Y.A. Ichou, Desalination 235 (2009) 264–275.
[3] D.V. Bavykin, K.E. Redmond, B.P. Nias, A.N. Kulak, F.C. Walsh, Aust. J. Chem. 63 (2010) 270–275.
[4] Y.C. Hsiao, T.F. Wu, Y.S. Wang, C.C. Hu, C. Huang, Appl. Catal. B: Environ. 148–149 (2014) 250–257.
[5] S. Zhang, Ceram. Int. 40 (2014) 4553–4557.
[6] V.S. Mane, I.D. Mall, V.C. Srivastava, J. Environ. Manage. 84 (2007) 390–400.
[7] C. Namasivayam, D. Kavitha, Dyes Pigment 54 (2002) 47–58.
[8] P.C. Vandevivere, R. Bianchi, W. Verstraete, J. Chem. Technol. Biotechnol. 72 (1998) 289–302.
[9] Y. Bayrak, R. Uzgor, Asian J. Chem. 25 (2013) 71–78.
[10] Z.F. Huang, J.J. Zou, L. Pan, S. Wang, X. Zhang, L. Wang, Appl. Catal. B: Environ. 147 (2014) 167–174.
[11] A. Naldoni, M. Allieta, S. Santangelo, M. Marelli, F. Fabbri, S. Cappelli, C.L. Bianchi, R. Psaro, V. Dal Santo, J. Am. Chem. Soc. 134 (2012) 7600–7603.
[12] P. Du, L. Song, J. Xiong, H. Cao, J. Mater. Sci. 48 (2013) 8386–8392.
[13] L. Yang, X. Jiang, W. Ruan, J. Yang, B. Zhao, W. Xu, J.R. Lombardi, J. Phys. Chem. C 113 (2009) 16226–16231.
[14] V. Vaiano, G. Iervolino, D. Sannino, L. Rizzo, G. Sarno, A. Farina, Appl. Catal. B: Environ. 160–161 (2014) 247–253.
[15] C. Belver, C. Adán, M. Fernández-García, Catal. Today 143 (2009) 274–281.
[16] N. Daneshvar, H. Ashassi-Sorkhabi, A. Tizpar, Sep. Purif. Technol. 31 (2003) 153–162.
[17] M. Hajaghazadeh, V. Vaiano, D. Sannino, H. Kakooei, R. Sotudeh-Gharebagh, P. Ciambelli, Catal. Today 230 (2014) 79–84.
[18] J.J. Murcia, M.C. Hidalgo, J.A. Navío, V. Vaiano, D. Sannino, P. Ciambelli, Catal. Today 209 (2013) 164–169.
[19] D. Sannino, V. Vaiano, P. Ciambelli, Res. Chem. Intermed. 39 (2013) 4145–4157.
[20] D. Sannino, V. Vaiano, G. Sarno, P. Ciambelli, Chem. Eng. Trans. 39 (2014) 499–504.
[21] V. Vaiano, D. Sannino, A.R. Almeida, G. Mul, P. Ciambelli, Catalysts 3 (2013) 978–997.
[22] M. Antoniadou, V. Vaiano, D. Sannino, P. Lianos, Chem. Eng. J. 224 (2013) 144–148.
[23] L. Rizzo, D. Sannino, V. Vaiano, O. Sacco, A. Scarpa, D. Pietrogiacomi, Appl. Catal. B: Environ. 144 (2014) 369–378.
[24] O. Sacco, M. Stoller, V. Vaiano, P. Ciambelli, A. Chianese, D. Sannino, Int. J. Photoenergy 2012 (2012).
[25] D. Sannino, V. Vaiano, O. Sacco, P. Ciambelli, J. Environ. Chem. Eng. 1 (2013) 56–60.
[26] V. Vaiano, O. Sacco, D. Sannino, P. Ciambelli, S. Longo, V. Venditto, G. Guerra, J. Chem. Technol. Biotechnol. 89 (2014) 1175–1181.
[27] V. Vaiano, O. Sacco, M. Stoller, A. Chianese, P. Ciambelli, D. Sannino, Int. J. Chem. React. Eng. 12 (2014).
[28] C. Han, M. Pelaez, V. Likodimos, A.G. Kontos, P. Falaras, K. O'Shea, D.D. Dionysiou, Appl. Catal. B: Environ. 107 (2011) 77–87.
[29] C. Guarisco, G. Palmisano, G. Calogero, R. Ciriminna, G. Di Marco, V. Loddo, M. Pagliaro, F. Parrino, Environ. Sci. Pollut. Res. 21 (2014) 1–7.
[30] Y. Zhang, R. Ciriminna, G. Palmisano, Y.J. Xu, M. Pagliaro, RSC Adv. 4 (2014) 18341–18346.
[31] M. Pelaez, N.T. Nolan, S.C. Pillai, M.K. Seery, P. Falaras, A.G. Kontos, P.S.M. Dunlop, J.W.J. Hamilton, J.A. Byrne, K. O'Shea, M.H. Entezari, D.D. Dionysiou, Appl. Catal. B 125 (2012) 331–349.
[32] R.L. Pozzo, M.A. Baltanás, A.E. Cassano, Catal. Today 39 (1997) 219–231.
[33] S. Singh, H. Mahalingam, P.K. Singh, Appl. Catal. A: Gen. 462–463 (2013) 178–195.
[34] I.K. Konstantinou, T.M. Sakellarides, V.A. Sakkas, T.A. Albanis, Environ. Sci. Technol. 35 (2001) 398–405.
[35] J. Kumar, A. Bansal, Int. J. Environ. Sci. Technol. 9 (2012) 479–484.
[36] D. Avisar, I. Horovitz, L. Lozzi, F. Ruggieri, M. Baker, M.L. Abel, H. Mamane, J. Hazard. Mater. 244–245 (2013) 463–471.
[37] D.-B. Lee, G.-Y. Kim, J.-K. Lee, Met. Mater. Int. 9 (2003) 43–46.
[38] K. Shankar, K.C. Tep, G.K. Mor, C.A. Grimes, J. Phys. D: Appl. Phys. 39 (2006) 2361–2366.
[39] M.C. Rosu, R.C. Suciu, I. Kasco, S.V. Dreve, E. Indrea, T.D. Silipas, J. Phys.: Conf. Ser. 182 (2009).
[40] Y. Wang, Y. Xie, J. Yuan, G. Liu, Asian J. Chem. 25 (2013) 739–744.
[41] J.C. Parker, R.W. Siegel, J. Mater. Res. 5 (1990) 1246–1252.
[42] W.S. Li, Z.X. Shen, H.Y. Li, D.Z. Shen, X.W. Fan, J. Raman Spectrosc. 32 (2001) 862–865.
R.K. Wahi, Y. Liu, J.C. Falkner, V.L. Colvin, J. Colloid Interface Sci. 302 (2006) 530–536.
[44] A. Soloviev, R. Tufeu, C. Sanchez, A.V. Kanaev, J. Phys. Chem. B 105 (2001) 4175–4180.
[45] Z.Z. Baros, B.K. Adnadevic, Russ. J. Phys. Chem. A 85 (2011) 2295–2298.
[46] M. Batzill, E.H. Morales, U. Diebold, Phys. Rev. Lett. 96 (2006).
[47] A.I. Kontos, A.G. Kontos, D.S. Tsoukleris, G.D. Vlachos, P. Falaras, Thin Solid Films 515 (2007) 7370–7375.
[48] J. Kumar, A. Bansal, Water Air Soil Pollut. 224 (2013) 1–11.
[49] N.M. Julkapli, S. Bagheri, S.B. Abd Hamid, Sci. World J. 2014 (2014) 692301–692326, 692307.